Published in final edited form as:
Nano Lett. 2014 February 12; 14(2): 972–981. doi:10.1021/nl404391r.

Passive vs. Active Tumor Targeting using RGD-and NGR-modified Polymeric Nanomedicines

Sijumon Kunjachan[1], **Robert Pola**[2], **Felix Gremse**[1], **Benjamin Theek**[1], **Josef Ehling**[1], **Diana Moeckel**[1], **Benita Hermanns-Sachweh**[3], **Michal Pechar**[2], **Karel Ulbrich**[2], **Wim E. Hennink**[4], **Gert Storm**[4,5], **Wiltrud Lederle**[1], **Fabian Kiessling**[1,*], and **Twan Lammers**[1,4,5,*]

[1]Dept. of Experimental Molecular Imaging, University Hospital and Helmholtz Institute for Biomedical Engineering, RWTH Aachen, Pauwelsstrasse 30, 52074 Aachen, Germany [2]Institute of Macromolecular Chemistry, Academy of Sciences of the Czech Republic, Heyrovsky Square 2, 162 06 Prague 6, Czech Republic [3]Electron Microscopy, Institute of Pathology, Medical Faculty, RWTH Aachen, Pauwelstrasse 30, 52074 Aachen, Germany [4]Dept. of Pharmaceutics, Utrecht Institute for Pharmaceutical Sciences, Utrecht University, Universiteitsweg 99, 3584 CG Utrecht, The Netherlands [5]Dept. of Controlled Drug Delivery, MIRA Institute for Biomedical Technology and Technical Medicine, University of Twente, PO Box 217, 7500 AE, Enschede, The Netherlands

Abstract

Enhanced permeability and retention (EPR), and the (over-) expression of angiogenesis-related surface receptors are key features of tumor blood vessels. As a consequence, EPR-mediated passive and RGD- and NGR-based active tumor targeting have received considerable attention in the last couple of years. Using several different in vivo and ex vivo optical imaging techniques, we here visualized and quantified the benefit of RGD- and NGR-based vascular vs. EPR-mediated passive tumor targeting. This was done using ~10 nm-sized polymeric nanocarriers, which were either labeled with DY-676 (peptide-modified polymers) or with DY-750 (peptide-free polymers). Upon co-injection into mice bearing both highly leaky CT26 and poorly leaky BxPC3 tumors, it was found that vascular targeting did work, resulting in rapid and efficient early binding to tumor blood vessels, but that over time, passive targeting was significantly more efficient, leading to higher overall levels and to more efficient retention within tumors. Although this situation might be different for larger carrier materials, these insights indicate that caution should be taken not to over-estimate the potential of active over passive tumor targeting.

Keywords

Nanomedicine; Drug targeting; EPR; RGD; NGR

Paralleled by the ever-increasing advances in nanotechnology and chemical engineering, nanomedicine formulations have started to attract significant attention in the last couple of years. Nanomedicines are 1-100(0) nm-sized carrier materials designed to improve the biodistribution and target site accumulation of low-molecular-weight (chemo-) therapeutic agents. By means of both passive and active targeting mechanisms, nanocarrier materials

[*]**Corresponding Authors** Prof. Dr. Fabian Kiessling; Tel: +49-241-8080116; fkiessling@ukaachen.de Dr. Dr. Twan Lammers; Tel: +49-241-8036681; tlammers@ukaachen.de.

Supporting Information Materials and methods describing the synthesis and characterization of the polymeric nanocarriers are provided as supplementary information. This material is available free of charge via the Internet at http://pubs.acs.org.

Europe PMC Funders Author Manuscripts

aim to more efficiently deliver drug molecules to pathological sites, while at the same time preventing their accumulation in potentially endangered healthy tissues, thereby beneficially affecting the balance between their efficacy and toxicity [1-4].

Passive drug targeting relies on the hyper-permeable tumor vasculature. Endothelial gaps and improperly aligned vascular endothelium result in leaky blood vessels, which enable the extravasation of carrier materials with sizes of up to several 100's of nm into the tumor interstitium. In addition to this, dysfunctional lymphatic drainage results in the retention of extravasated nanomaterials within tumorous tissues. Together, these two pathophysiological features give rise to the 'Enhanced Permeability and Retention' (EPR) effect, which is extensively used in the nanomedicine field [5,6]. Several EPR-targeted nanomedicines, such as Doxil (PEGylated liposomal doxorubicin), Myocet (non-PEGylated liposomal doxorubicin) and DaunoXome (non-PEGylated liposomal daunorubicin) are routinely used in patients, and many others are currently in (pre-) clinical trials [7-9].

It is important to keep in mind in this regard that EPR is a highly variable phenomenon, characterized by large inter- and intra- individual differences [5,10-14]. Not only do EPR-determining parameters, such as vascular volume, perfusion, permeability, penetration and retention, differ quite significantly between different types of tumors, they generally also differ between different tumors within the same patient. And actually even within a single tumor, certain vessels are more permeable and/or better perfused than others, together resulting in very heterogeneous EPR. In general, both in animal models and in patients, rapidly growing and highly vascularized tumors tend to be more permeable than slowly growing and poorly vascularized tumors, thereby making them more prone to EPR-mediated passive drug targeting. This can be exemplified by taking into account that Kaposi sarcoma tumors, which are known to be highly vascularized and highly leaky, accumulate long-circulating liposomes very efficiently [15], and respond very well to treatment with Doxil, doubling response rates as compared to the triple chemotherapy combination Adriamycin (Doxorubicin), Bleomycin and Vincristine [16]. Vice versa, patients suffering from less-permeable tumors, such as the vast majority of breast carcinomas [15], did not really benefit from Doxil vs. free doxorubicin treatment. Progression-free and overall survival times were found to be similar for the liposomal and the free drug, but the toxicity profile was beneficially affected, with less bone marrow depression, alopecia, nausea and vomiting, and with a shift of the dose-limiting toxicity from cumulative cardiomyopathy for free doxorubicin to hand-and-foot syndrome for Doxil [16-18].

As opposed to passive drug targeting, which essentially only relies on the pathophysiological properties of target tissue and on the prolonged circulation time of nanocarriers, active targeting is based on the incorporation of specific recognition motifs within nanomedicine formulations. Examples of routinely used targeting ligands are antibodies, peptides, nanobodies, sugar molecules and aptamers. These entities aim to specifically bind to cell surface or matrix molecules present in high amount at the target site, which in case of tumors generally refers to receptors highly (over-) expressed either by the cancer cells themselves (e.g. EGFR or PSMA), or by tumor endothelial cells (e.g. VEGFR2 or integrins) [11,19-23].

In the last decade, a significant number of drug targeting studies have focused on the synthesis and evaluation of actively targeted nanomedicines, primarily aiming to deliver higher payloads of drugs to tumors over time. Strikingly, however, in spite of often highly promising in vitro findings, showing e.g. enhanced binding, uptake, intracellular processing and efficacy, only a relatively small number of studies have managed to demonstrate that active targeting of nanocarriers really helps to improve their in vivo tumor

accumulation [24-31]. Consequently, scrutiny has risen in recent years with regard to the potential of active over passive tumor targeting.

In light of this, it has become apparent that in particular in case of active targeting to cancer cells, extravasation from the vascular compartment into tumor interstitium is the rate-limiting step for efficient site-specific drug delivery. This, together with the fact that I) the intratumoral penetration of nanomaterials with sizes exceeding ~10 nm tends to be poor [32-34] and that II) the presence of targeting ligands on the surface of nanocarriers generally has deleterious pharmacokinetic consequences (reducing their circulation half-life times and their passive EPR-mediated accumulation in tumors [11,27,29]), calls for a systematic analysis of the benefit of active versus passive tumor targeting. Surely, under certain circumstances, e.g. in case of DNA or siRNA delivery, where cellular internalization by a specific target cell population within a solid tumor is absolutely necessary, active targeting is imperative [35-37]. Similarly, also in situations in which the targeting ligand contributes to the overall pharmacological activity of the developed nanomedicine formulation, e.g. in case of Erbitux-modified Doxil, Acupa-modified docetaxel nanoparticles and anti-EGFR-nanobody-modified polymeric micelles carrying doxorubicin, ‘active targeting’ has been shown to be beneficial, significantly improving therapeutic outcome as compared to passively targeted controls lacking such potentially therapeutic targeting ligands [38-41]. This improved efficacy, however, most likely does not result from improved tumor accumulation upon ‘active targeting’, but from additive or even synergistic interactions at the cellular and molecular level.

Given the fact that hardly any systematic comparisons are available addressing the potential of active vs. passive tumor targeting, we here longitudinally visualized and quantified the tumor accumulation of RGD- and NGR-based polymeric nanocarriers, and compared it to that of DRG- and peptide-free control copolymers. RGD- and NGR-containing oligopeptides bind to integrin ($\alpha_v\beta_3$) and aminopeptidase N (CD13) receptors, and are routinely used ligands for active targeting to tumor blood vessels [42,43]. As depicted schematically in Figure 1, we prepared prototypic ~10 nm-sized polymeric drug carriers based on poly(N-(2-hydroxypropyl)methacrylamide) (i.e. pHPMA; which has been extensively evaluated both in animal models and in patients [17,22,44-47]), and we labeled the peptide-containing and the peptide-free polymers with two different near-infrared fluorophores (i.e. DY-676 and DY-750, respectively). The two probes were then co-injected into tumor-bearing mice, in order to reduce animal-to-animal and tumor-to-tumor variability. Biodistribution and tumor accumulation were longitudinally monitored for up to 72 h, using 2D fluorescence reflectance imaging (FRI) and 3D computed tomography-fluorescence molecular tomography (CT-FMT) [48,49]. Two different mouse models were employed, i.e. rapidly growing and highly leaky CT26 mouse colorectal carcinoma tumors, and slowly growing and much less leaky BxPC3 human pancreatic carcinoma tumors. As exemplified by Figure 1C, we predicted that the added value of active vascular targeting over EPR-mediated passive targeting would depend on the baseline level of vascular leakiness. In case of poorly leaky tumors, there are good reasons to believe that vascular targeting might work (at least for a certain period of time), whereas in cases of highly leaky tumors, passive targeting likely dominates. This is because actively targeted nanocarriers, such as antibody-modified liposomes or peptide-modified polymers, generally circulate shorter than their passively targeted counterparts. As a result of this, they tend to be somewhat less suitable for EPR-mediated passive drug targeting. Largely in line with this reasoning, the findings described below demonstrate that in case of ~10 nm-sized polymeric carrier materials, RGD- and NGR-based vascular targeting does work, leading to rapid and relatively efficient early binding to tumor blood vessels, but does not increase the long-term levels of model drug molecules accumulating in tumors over time. Although this situation might be different for other (in particular larger) drug delivery systems, these findings

indicate that the potential of active over passive tumor targeting should not be over-estimated.

The passively and actively targeted polymeric nanocarriers P-CON, P-DRG, P-RGD and P-NGR were synthesized using previously established procedures (see supplementary materials and methods section for details). As shown in Figure 2A, P-CON did not contain a peptide fragment, and was labeled with the near-infrared fluorophore (NIRF) DY-750. P-RGD, P-NGR and P-DRG were labeled with the NIRF DY-676, and were coupled to the cyclic pentapeptides cyclo(RGDfK), cyclo(CNGRC) and cyclo(DRfGK), via a short PEG-based spacer (Figure 2A). The average molecular weight of the polymeric nanocarriers was ~70 kD, their polydispersity index was ~1.6, their dye content was 2.3% w/w, and their peptide-content was 8-9% w/w (Figure 2B). The optical properties of purified constructs were assessed spectrophotometrically and using fluorescence molecular tomography (FMT; Figure 2C). The relative signal intensities in the phantoms were used to calibrate the FMT device for the in vivo experiments.

Two-dimensional fluorescence reflectance imaging (2D FRI) was employed to evaluate the early binding kinetics of the peptide-targeted polymers to tumor blood vessels, as well as their long-term retention within tumors. To minimize the impact of inter-individual variability, the DY-750-labeled control copolymer P-CON was co-injected together with the peptide-modified DY-676-labeled copolymers P-RGD, P-NGR and P-DRG into the same CT26 and BxPC3 tumor-bearing mice. As exemplified by Figure 3, non-invasive 2D FRI at early (0.25, 0.5, 1 and 4 h) and late (24, 48 and 72 h) time points after i.v. injection clearly demonstrated that both P-RGD and P-NGR rapidly and efficiently bound to integrin ($\alpha_v\beta_3$) and aminopeptidase N (CD13) receptors on activated tumor endothelium. In case of the passively targeted probes P-DRG and P-CON, there were no signs of early binding and rapid tumor localization. Instead, there was a progressive EPR-mediated tumor accumulation, which started to become apparent from 24 h onwards in the 2D FRI images (Figure 3). As expected, the EPR-mediated accumulation of the probes was found to be much stronger in rapidly growing CT26 tumors (~8 mm in ~2 weeks) than in slowly growing BxPC3 tumors (~8 mm in ~6 months). Interestingly, however, in spite of these very different growth kinetics and differences in EPR-mediated tumor localization, vascular targeting appeared to be equally efficient in both models, with very prominent early binding already detectable from 15 min onwards, and with no obvious overall difference in the degree of vascular tumor targeting. However, it has to be kept in mind in this regard that 2D FRI has light depth- and penetration-dependent limitations in quantitatively assessing nanomedicine-based tumor targeting and biodistribution [48]. Consequently, these results should at best be considered as semi-quantitative, providing valuable feedback on the kinetics of tumor targeting, but not its on overall efficiency (in particular since a direct quantitative comparison of the fluorescence intensity at 680 and 750 nm is impossible).

To overcome the abovementioned shortcoming with regard to quantitatively comparing the tumor accumulation of the different NIRF-labeled nanocarriers [48,50], and to at the same time allow for non-invasive whole-body biodistribution analyses (which are impossible using FRI, given the poor penetration depth of light), we recently established a hybrid imaging technique based on the combination of microcomputed tomography (CT) and fluorescence molecular tomography (FMT). In CT-FMT, the quantitative 3D fluorescence information obtained using FMT is merged with the respective μCT images of the whole mouse, and the fluorescent clouds corresponding to probe accumulation can be allocated to both superficial (tumor) lesions and to deeper-seated healthy organs and tissues. This hybrid imaging technique is therefore considered to be highly valuable for nanomedicine research, combining the high sensitivity of optical imaging, which has a detection limit in the order of

nano- to picomoles, with the very high spatial resolution of μCT imaging, which in small animals can narrow down to several tens of micrometers [48,50,51].

To extend the results obtained using 2D FRI, we therefore also employed 3D CT-FMT to compare vascular vs. passive targeting in mice bearing CT26 and BxPC3 tumors, enabling not only the direct visualization of the target site accumulation of P-RGD, P-NGR, P-DRG and P-CON, but also their quantification. Exemplary images of mice at early (1 h) and late (48 h) time points after i.v. injection clearly show that in line with the data obtained using 2D-FRI, rapid tumor localization was observed for P-RGD and P-NGR in both CT26 and BxPC3 tumors (Figure 4A). In contrast, P-DRG and P-CON were barely detectable within tumors at this early time point. At later stages (48 h), however, this situation was found to be reversed, with hardly any probe accumulation detectable for P-RGD and P-NGR, but with very prominent EPR-mediated passive tumor targeting for P-DRG and P-CON (Figure 4A). 3D CT-FMT-based quantifications confirmed these observations, showing a peak in P-RGD and P-NGR tumor accumulation at 1 h, which leveled off at ~50% of the initial peak concentration at later time points (Figure 4B). Both untargeted probes, i.e. P-DRG and P-CON, did not display signs of early binding, but gradually accumulated in tumors over time, in line with the basic principles of EPR. Interestingly, but not unexpectedly, the incorporation of the scrambled DRG peptide resulted in less efficient EPR (~50% lower overall tumor AUC as compared to P-CON), likely due to the slightly less stealthy character of the peptide-modified polymer, leading to a somewhat more rapid elimination via the reticuloendothelial system (RES; nowadays generally referred to as MPS, i.e. mononuclear phagocytic system) [52].

Equally interestingly, no large differences between P-RGD and P-NGR were observed in leaky vs. non-leaky tumors: in both cases, a peak concentration of 2-3% of the injected dose (%ID) was found to accumulate at the target site at 1 h post i.v. injection. When comparing the levels of the two passively targeted polymer conjugates P-DRG and P-CON in both tumor models, a clear impact of tumor growth kinetics and vascular leakiness on the overall extent of tumor accumulation was detectable, with almost twice as high concentrations of the carrier materials accumulating in CT26 tumors (Figure 4B). For P-CON, for instance, a plateau concentration of more than 6 %ID was achieved between 24 and 72 h p.i. in CT26 tumors, whereas in BxPC3 tumors, long-term levels plateaued at ~3 %ID. Together, these findings indicate that independent of the tumor model used, EPR-mediated passive drug targeting outperforms RGD- and NGR-based active targeting to tumor blood vessels, at least in case of ~10 nm-sized macromolecular carrier materials.

At 72 h p.i., the animals were sacrificed, tumors were harvested and findings were validated ex vivo. As shown in Figure 5A-B, in line with results obtained using in vivo CT-FMT, EPR-mediated passive targeting using P-CON resulted in much higher levels of tumor accumulation than did active (vascular) targeting using P-RGD and P-NGR. In line with the concept put forward in Figure 1, these differences appeared to be somewhat larger in CT26 than in BxPC3, but one has to keep in mind in this regard that these 2D FRI results are at best semi-quantitative. As exemplified by Figure 5C, we also analyzed the ex vivo biodistribution of the four probes, showing that the modification of the polymeric carrier materials with peptides increases their off-target accumulation in healthy organs. This notion is in line with previously published reports, in which radionuclide-based imaging techniques were employed to demonstrate that upon conjugating peptides to polymers, their long-circulating properties decrease, and their levels accumulating in healthy non-target tissues, in particular in kidney, liver and spleen, are increased [20,49,52,53]. In addition to the fact that the beneficial impact of active targeting to tumor blood vessels is relatively short-lived (Figure 4A-B), these deleterious biodistributional consequences of modifying polymers with

peptides (Figure 5C) explain why RGD- and NGR-targeted nanocarriers do not accumulate as efficiently in tumors as do their unmodified counterparts.

Excised tumors were subsequently evaluated using immunohistochemistry (IHC). As shown in Figure 6, the degree of co-localization between the polymeric probes and tumor blood vessels was assessed. To this end, sections were stained using antibodies against the blood vessel marker CD31, and images were fused with those obtained for the DY-676-labeled polymers. In good agreement with the observed early accumulation of P-RGD and P-NGR in CT26 and BxPC3 tumors (Figures 3 and 4), which is indicative of efficient binding to tumor blood vessels, significantly higher levels of overlap were observed between P-RGD and P-NGR and CD31, as compared to P-DRG and CD31 (Figure 6B). Interestingly, in BxPC3, the degree of P-RGD and P-NGR co-localization was approximately twice as high as in CT26 tumors, which might explain why the difference between active and passive targeting appeared to be somewhat smaller in BxPC3, in particular in direct comparison to P-DRG (cf. Figures 4B and 5B). In line with the in vivo results and with the literature [26-28,30,54,55], these microscopy findings verify that RGD and NGR can be used to target specific surface receptors (over-) expressed by tumor blood vessels, but also that in case of ~10 nm-sized macromolecular carrier materials, this does not lead to improved and/or prolonged tumor accumulation. Vascular targeting does clearly alter the kinetics of tumor targeting, with prominent early binding (Figures 3, 4) and with significantly more co-localization at the microscopy level (Figure 6), but when it comes to achieving optimal drug delivery efficiency, i.e. high concentrations for prolonged periods of time, passive drug targeting appears to be the method of choice for such relatively small polymeric drug carriers.

Finally, to verify that differences in vascular permeability are primarily responsible for the observed differences in tumor accumulation in CT26 vs. BxPC3 tumors, we visualized and quantified vascular leakiness in these two models. As shown in Figure 7, this was done using the Evans Blue Dye (EBD) extravasation assay, as well as high-resolution transmission (TEM) and scanning electron microscopy (SEM). EBD is a well-known vascular permeability marker [56,57]. It strongly binds to serum albumin and can therefore be used to qualitatively and quantitatively assess albumin extravasation [13,57]. In agreement with their much more rapid in vivo growth kinetics, with the passive targeting results presented in Figures 3-5, and with the α-SMA expression levels presented in Figure S1, it was observed that CT26 tumors displayed much higher levels of vascular leakiness than did BxPC3 tumors (Figure 7A). Extraction of EBD and spectrophotometric quantification confirmed this notion, showing a 2-3-fold higher level of albumin extravasation in CT26 (Figure 7B), which is in line with the 2-3-fold higher accumulation of P-CON and P-DRG in CT26 (Figure 4B). These insights were extended using TEM and SEM, illustrating that CT26 tumors presented with more disorganized and more defective blood vessel morphologies, such as larger perforations and larger variations in pericyte coverage (Figure 7C). Endothelial misalignment and lack of proper endothelial coverage were relatively frequently observed in CT26, and were less common in BxPC3 tumors. For healthy control tissue (kidney), a well-organized and highly uniform endothelial lining was observed. High-resolution SEM imaging revealed several clearly discernible pores in the capillaries in CT26 tumors, with sizes of up to 150 nm, which were not observed in BxPC3 tumors (Figure 7D-F). These observations are in line the EBD extravasation studies and confirm the notion that EPR-mediated passive drug targeting is significantly more efficient in CT26 than in BxPC3 tumors.

In summary, in two different tumor models with varying degrees of vascular leakiness. we systematically compared EPR-mediated passive vs. RGD- and NGR-based active tumor targeting for ~10 nm-sized polymeric drug carriers (Figures 1, 2 and 7). We show that RGD-

and NGR-based active targeting does work, resulting in rapid and relatively specific binding to tumor blood vessels, but also that peptide-targeting is inferior to standard EPR-mediated passive drug targeting when it comes to delivering high amounts of model drugs to tumors over time (Figures 3-6). In line with the literature, polymeric drug carriers with a size of ~10 nm presented with prominent EPR-mediated passive tumor targeting. Arguably, carrier materials with a size of ~10 nm are optimal for achieving proper tumor accumulation and tumor penetration, as they are sufficiently large to prevent rapid renal excretion, and at the same time also sufficiently small to extravasate from tumor blood vessels and penetrate into the highly dense tumor interstitium. Consequently, even in poorly leaky BxPC3 tumors, a significant amount of P-CON accumulated over time via EPR, and since peptide-modification negatively affected the biodistribution of the polymers (Figure 5), EPR-mediated passive targeting prevailed over RGD- and NGR-mediated active targeting in both CT26 and BxPC3 tumors (Figures 3-5).

This situation might be different for different types of tumors and different nanocarrier formulations. Regarding the former, as exemplified by Figure 1C, the benefit of active vascular targeting likely increases with decreasing vascular leakiness. As a result of this, it is expected that in tumors growing even slower than BxPC3 xenografts, as well as in the majority of human tumors (which tend to be much less leaky than mouse tumors), RGD- and NGR-modified nanocarriers might perform better than in the two tumor models used here. Regarding the latter, two parameters are expected to play a key role, i.e. nanocarrier size and the impact of the targeting ligand on the pharmacokinetics and the biodistribution of the carrier material. The nature of the carrier material, on the other hand, does not necessarily play a role, as long as the physicochemical and ‘immunological’ properties of the employed drug delivery system enable it to circulate for prolonged periods of time, and to passively accumulate in tumors via EPR.

Nanocarrier size is directly related to the pore cutoff-size of tumor blood vessels. It therefore seems logical that the larger the carrier material is, the more likely it is to benefit from vascular targeting. There might for instance be tumors (with the majority of endothelial pores larger than 10 nm and smaller than 100 nm) in which ~10 nm-sized RGD- and NGR-targeted polymers fail to improve tumor accumulation as compared to passively targeted polymers, but in which ~100 nm-sized RGD- or NGR-targeted liposomes do show a clear benefit. This notion can be exemplified by taking into account that microbubbles (i.e. 1-5 μm-sized gas- or air-filled vesicles routinely used as contrast agents for ultrasound imaging) do not accumulate at all within tumors via EPR, as they are far too large to extravasate from the tumor vasculature. Upon vascular targeting, however, i.e. upon modifying the polymer- or lipid-based microbubble surface with antibodies or peptides recognizing receptors overexpressed by tumor blood vessels (e.g. VEGFR2 or integrins), significant numbers of microbubbles are retained within tumors, rendering them useful for molecular imaging and tumor-targeted drug delivery purposes [58-60].

The second key issue determining the potential added value of active vascular targeting over EPR-mediated passive targeting is the impact of the targeting ligand on the circulation kinetics of the carrier material. Theoretically, if the presence of targeting ligands would not lead to a shorter circulation half-life time and/or to an increase in off-target localization, actively targeted nanocarriers would profit as efficiently from EPR as would passively targeted formulations. Consequently, they would achieve at least similar (and likely even higher; because of enhanced early binding) overall levels of tumor accumulation. In the vast majority of cases, however, conjugating targeting ligands to long-circulating nanocarriers has a profound effect on their pharmacokinetics and their biodistribution, and it often significantly lowers their ability to exploit EPR. This is particularly relevant for cancer cell-targeted nanomedicines, which have to accumulate in tumors first via enhanced

permeability, before they can be more efficiently retained there via active targeting (e.g. via enhanced cellular uptake). This situation is different for endothelial cell-targeted nanocarriers, for which overall levels of tumor accumulation depend on the sum of relatively rapid endothelial binding plus relatively slow EPR-mediated extravasation. The latter notion implies that also in the case of active targeting to tumor blood vessels, it is important to ensure that the presence of targeting ligands does not negatively affect the pharmacokinetics and the biodistribution of long-circulating nanomedicines (at least not too much).

Taken together, the above insights and efforts demonstrate that modifying ~10 nm-sized polymeric drug carriers with RGD- and NGR-based oligopeptides enables active targeting to tumor blood vessels, as exemplified by efficient in vivo target site accumulation in the first few hours after i.v. administration, and by prominent ex vivo colocalization with angiogenic endothelial cells. The long-term levels of RGD-and NGR-modified carrier materials, however, were found to be lower than those of unmodified control copolymers. These findings indicate that in case of long-circulating nanomedicine formulations, the potential of active over passive tumor targeting should not be over-estimated.

Supplementary Material

Refer to Web version on PubMed Central for supplementary material.

Acknowledgments

This work was supported by the European Research Council (ERC Starting Grant 309495: NeoNaNo), by the German Federal State of North Rhine Westphalia (NRW; HighTech.NRW / EU-Ziel 2-Programm (EFRE); ForSaTum), by the European Union (European Regional Development Fund-Investing In Your Future; and COST-Action TD1004-Nanotheragnostics), by the German Research Foundation (DFG; LA2937/1-2) and by the Grant Agency of the Czech Republic (grant No. P207/12/J030).

References

1. Farokhzad OC, Langer R. ACS Nano. 2009; 3:16–20. [PubMed: 19206243]
2. Allen TM, Cullis PR. Science. 2004; 303:1818–1822. [PubMed: 15031496]
3. Peer D, Karp JM, Hong S, Farokhzad OC, Margalit R, Langer R. Nat. Nanotechnol. 2007; 2:751–760. [PubMed: 18654426]
4. Davis ME, Chen Z, Shin DM. Nat Rev Drug Discov. 2008; 7:771–782. [PubMed: 18758474]
5. Matsumura Y, Maeda H. Cancer Res. 1986; 46:6387–6392. [PubMed: 2946403]
6. Maeda H. J. Control. Release. 2012; 164:138–144. [PubMed: 22595146]
7. Lammers T, Hennink WE, Storm G. Br J Cancer. 2008; 99:392–397. [PubMed: 18648371]
8. Jain RK, Stylianopoulos T. Nature Reviews Clinical Oncology. 2010; 7:653–654.
9. Barenholz Y. J Control Release. 2012; 160:117–134. [PubMed: 22484195]
10. Prabhakar U, Maeda H, Jain RK, Sevick-Muraca EM, Zamboni W, Farokhzad OC, Barry ST, Gabizon A, Grodzinski P, Blakey DC. Cancer Res. 2013; 73:2412–2417. [PubMed: 23423979]
11. Lammers T, Kiessling F, Hennink WE, Storm G. J. Control. Release. 2012; 161:175–187. [PubMed: 21945285]
12. Greish K. Methods Mol. Biol. 2010; 624:25–37. [PubMed: 20217587]
13. Taurin S, Nehoff H, Greish K. J. Control. Release. 2012; 164:265–275. [PubMed: 22800576]
14. Smith BR, Kempen P, Bouley D, Xu A, Liu Z, Melosh N, Dai H, Sinclair R, Gambhir SS. Nano Lett. 2012; 12:3369–3377. [PubMed: 22650417]
15. Harrington KJ, Mohammadtaghi S, Uster PS, Glass D, Peters AM, Vile RG, Stewart JS. Clin. Cancer Res. 2001; 7:243–254. [PubMed: 11234875]
16. Northfelt DW, Dezube BJ, Thommes JA, Miller BJ, Fischl MA, Friedman-Kien A, Kaplan LD, Du Mond C, Mamelok RD, Henry DH. J. Clin. Oncol. 1998; 16:2445–2451. [PubMed: 9667262]

17. O'Brien MER, Wigler N, Inbar M, Rosso R, Grischke E, Santoro A, Catane R, Kieback DG, Tomczak P, Ackland SP, Orlandi F, Mellars L, Alland L, Tendler C, CAELYX Breast Cancer Study Group. Ann. Oncol. 2004; 15:440–449. [PubMed: 14998846]
18. Lammers T, Rizzo LY, Storm G, Kiessling F. Clin Cancer Res. 2012; 18:4889–4894. [PubMed: 22829203]
19. Pasqualini R, Koivunen E, Ruoslahti E. Nat. Biotechnol. 1997; 15:542–546. [PubMed: 9181576]
20. Line BR, Mitra A, Nan A, Ghandehari H. J. Nucl. Med. 2005; 46:1552–1560. [PubMed: 16157540]
21. Zhang C, Jugold M, Woenne EC, Lammers T, Morgenstern B, Mueller MM, Zentgraf H, Bock M, Eisenhut M, Semmler W, Kiessling F. Cancer Res. 2007; 67:1555–1562. [PubMed: 17308094]
22. Pola R, Studenovsky M, Pechar M, Ulbrich K, Hovorka O, Vetvicka D, Rihova B. J Drug Target. 2009; 17:763–766. [PubMed: 19863198]
23. Fokong S, Theek B, Wu Z, Koczera P, Appold L, Jorge S, Resch-Genger U, van Zandvoort M, Storm G, Kiessling F, Lammers T. J. Control. Release. 2012; 163:75–81. [PubMed: 22580225]
24. Kirpotin DB, Drummond DC, Shao Y, Shalaby MR, Hong K, Nielsen UB, Marks JD, Benz CC, Park JW. Cancer Res. 2006; 66:6732–6740. [PubMed: 16818648]
25. Choi CH, Alabi CA, Webster P, Davis ME. Proc Natl Acad Sci USA. 2010; 107:1235–40. [PubMed: 20080552]
26. Chen W, Jarzyna PA, van Tilborg GAF, Nguyen VA, Cormode DP, Klink A, Griffioen AW, Randolph GJ, Fisher EA, Mulder WJM, Fayad ZA. FASEB J. 2010; 24:1689–1699. [PubMed: 20075195]
27. Huang X, Peng X, Wang Y, Wang Y, Shin DM, El-Sayed MA, Nie S. ACS Nano. 2010; 4:5887–5896. [PubMed: 20863096]
28. Gianella A, Jarzyna PA, Mani V, Ramachandran S, Calcagno C, Tang J, Kann B, Dijk WJR, Thijssen VL, Griffioen AW, Storm G, Fayad ZA, Mulder WJM. ACS Nano. 2011; 5:4422–4433. [PubMed: 21557611]
29. Chattopadhyay N, Fonge H, Cai Z, Scollard D, Lechtman E, Done SJ, Pignol JP, Reilly RM. Mol. Pharmaceutics. 2012; 9:2168–2179.
30. Prokopiou EM, Ryder SA, Walsh JJ. Angiogenesis. 2013; 16:503–524. [PubMed: 23543223]
31. Salvati A, Pitek AS, Monopoli MP, Prapainop K, Bombelli FB, Hristov DR, Kelly PM, Aberg C, Mahon E, Dawson KA. Nat Nano. 2013; 8:137–143.
32. Wong C, Stylianopoulos T, Cui J, Martin J, Chauhan VP, Jiang W, Popovic Z, Jain RK, Bawendi MG, Fukumura D. Proc. Natl. Acad. Sci. 2011; 108:2426–2431. [PubMed: 21245339]
33. Popovic Z, Liu W, Chauhan VP, Lee J, Wong C, Greytak AB, Insin N, Nocera DG, Fukumura D, Jain RK, Bawendi MG. Angew. Chem. Int. Ed Engl. 2010; 49:8649–8652. [PubMed: 20886481]
34. Cabral H, Matsumoto Y, Mizuno K, Chen Q, Murakami M, Kimura M, Terada Y, Kano MR, Miyazono K, Uesaka M, Nishiyama N, Kataoka K. Nat Nano. 2011; 6:815–823.
35. Medarova Z, Pham W, Farrar C, Petkova V, Moore A. Nat. Med. 2007; 13:372–377. [PubMed: 17322898]
36. Ozpolat B, Sood AK, Lopez-Berestein G. J Intern. Med. 2010; 267:44–53. [PubMed: 20059643]
37. Davis ME. Mol. Pharm. 2009; 6:659–668. [PubMed: 19267452]
38. Hrkach J, Von Hoff D, Mukkaram Ali M, Andrianova E, Auer J, Campbell T, De Witt D, Figa M, Figueiredo M, Horhota A, et al. Sci Transl Med. 2012; 4:1–11.
39. Talelli M, Oliveira S, Rijcken CJF, Pieters EHE, Etrych T, Ulbrich K, van Nostrum RCF, Storm G, Hennink WE, Lammers T. Biomaterials. 2013; 34:1255–1260. [PubMed: 23122804]
40. Mamot C, Ritschard R, Wicki A, Stehle G, Dieterle T, Bubendorf L, Hilker C, Deuster S, Herrmann R, Rochlitz C. Lancet Oncol. 2013; 13:1234–1241. [PubMed: 23153506]
41. Gao J, Chen K, Luong R, Bouley DM, Mao H, Qiao T, Gambhir SS, Cheng Z. Nano Lett. 2011; 12:281–286. [PubMed: 22172022]
42. Temming K, Schiffelers RM, Molema G, Kok RJ. Drug Resist. Updat. 2005; 8:381–402. [PubMed: 16309948]
43. Corti A, Curnis F. Curr Pharm Biotech. 2011; 12:1128–1134.

44. Duncan R, Vicent MJ. Adv. Drug Deliv. Rev. 2010; 62:272–282. [PubMed: 20005271]
45. Lammers T, Ulbrich K. Adv. Drug Deliv. Rev. 2010; 62:119–121. [PubMed: 20005273]
46. Kopecek J, kopeckova P. Adv. Drug Deliv. Rev. 2010; 62:122–149. [PubMed: 19919846]
47. Lammers T, Subr V, Ulbrich K, Peschke P, Huber PE, Hennink WE, Storm G. Biomaterials. 2009; 30:3466–3475. [PubMed: 19304320]
48. Kunjachan S, Gremse F, Theek B, Koczera P, Pola R, Pechar M, Etrych T, Ulbrich K, Storm G, Kiessling F, Lammers T. ACS Nano. 2013; 7:252–262. [PubMed: 23067565]
49. Chytil P, Hoffmann S, Schindler L, Kostka L, Ulbrich K, Caysa H, Mueller T, Maeder K, Etrych T. J Control Release. 2013
50. Ale A, Ermolayev V, Herzog E, Cohrs C, de Angelis MH, Ntziachristos V. Nat. Methods. 2012; 9:615–620. [PubMed: 22561987]
51. Schulz RB, Ale A, Sarantopoulos A, Freyer M, Soehngen E, Zientkowska M, Ntziachristos V. IEEE Trans Med Imaging. 2010; 29:465–473. [PubMed: 19906585]
52. Lammers T, Kuhnlein R, Kissel M, Subr V, Etrych T, Pola R, Pechar M, Ulbrich K, Storm G, Huber P, Peschke P. J. Control. Release. 2005; 110:103–118. [PubMed: 16274831]
53. Etrych T, Subr V, Strohalm J, Sirova M, Rihova B, Ulbrich K. J. Control. Release. 2012; 164:346–354. [PubMed: 22759979]
54. Sugahara KN, Teesalu T, Karmali PP, Kotamraju VR, Agemy L, Girard OM, Hanahan D, Mattrey RF, Ruoslahti E. Cancer Cell. 2009; 16:510–520. [PubMed: 19962669]
55. Zhen Z, Tang W, Chen H, Lin X, Todd T, Wang G, Cowger T, Chen X, Xie J. ACS Nano. 2013; 7:4830–4837. [PubMed: 23718215]
56. Duncan R, Sat-Klopsch YN, Burger AM, Bibby MC, Fiebig HH, Sausville EA. Cancer Chemother. Pharmacol. 2013
57. Yao J, Maslov K, Hu S, Wang LV. J Biomed Opt. 2009; 14:054049. [PubMed: 19895150]
58. Hernot S, Klibanov AL. Adv. Drug Deliv. Rev. 2008; 60:1153–1166. [PubMed: 18486268]
59. Kiessling F, Fokong S, Koczera P, Lederle W, Lammers T. J. Nucl. Med. 2012; 53:345–348. [PubMed: 22393225]
60. Kiessling F, Fokong S, Bzyl J, Lederle W, Palmowski M, Lammers T. Adv. Drug Deliv. Rev. 2014 in press, DOI: 10.1016/j.addr.2013.11.013.

Europe PMC Funders Author Manuscripts

Europe PMC Funders Author Manuscripts

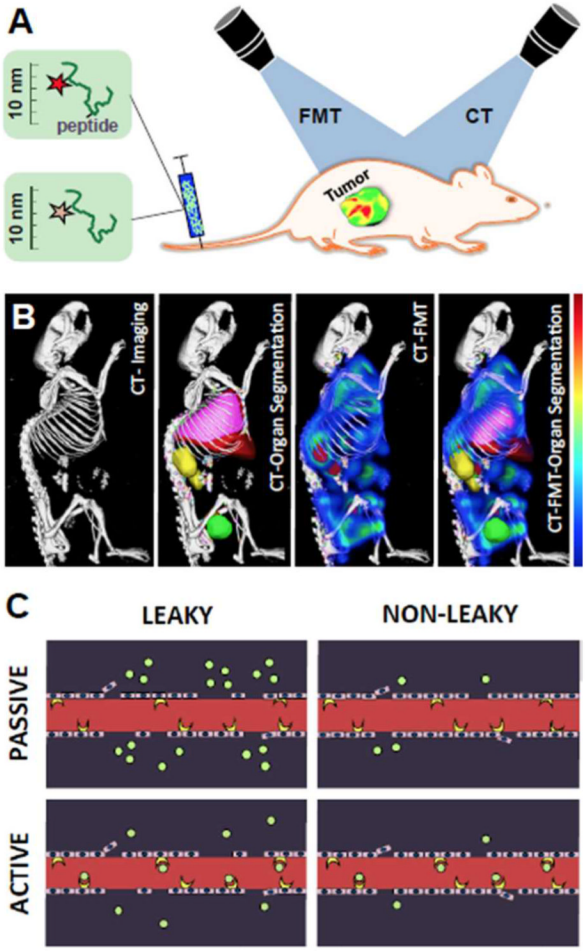

Figure 1. Monitoring EPR-mediated passive vs. RGD- and NGR-mediated active (vascular) tumor targeting

A. Schematic experimental setup, illustrating the co-injection of RGD- or NGR-modified polymeric nanocarriers (labeled with DY-676) together with unmodified control copolymers (labeled with DY-750). The carriers were co-injected into mice bearing either highly leaky CT26 tumors or poorly leaky BxPC3 tumors, and their tumor accumulation was visualized using 2D Fluorescence Reflectance Imaging (FRI) and hybrid 3D computed tomography-fluorescence molecular tomography (CT-FMT). B. Representative depiction of hybrid CT-FMT imaging, in which the anatomical information obtained using CT is used to properly allocate (and quantify) the tumor accumulation of the fluorophore-labeled nanocarriers. C. Schematic depiction of the potential benefit of active (vascular) targeting over EPR-mediated passive targeting in case of ~10 nm-sized polymeric drug carriers, exemplifying that in particular in case of non-leaky tumors, active vascular targeting might be beneficial. Note that actively targeted nanomedicines generally circulate somewhat shorter than passively targeted nanomedicines, and that this reduced plasma residence time results in somewhat lower amounts accumulating in tumors via EPR.

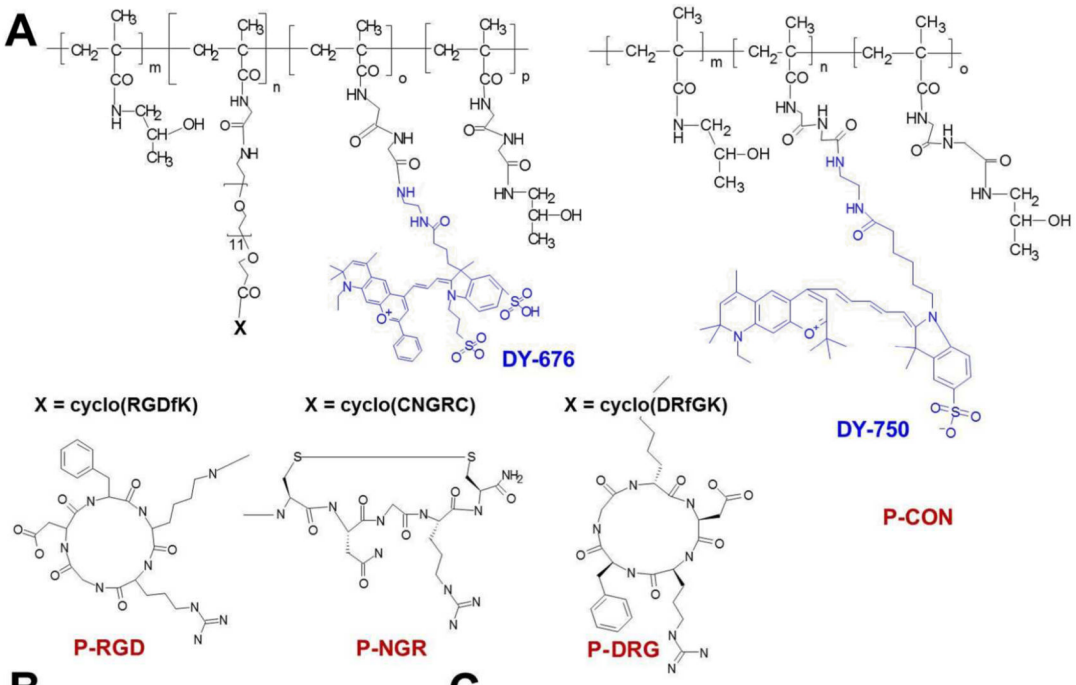

B

Polymeric Nanocarrier	MW (kDa)	PI (M_w/M_n)	Peptide (%)
P-RGD	70	1.6	8.3
P-NGR	67	1.5	8.8
P-DRG	71	1.6	9.1
P-CON	67	1.7	---

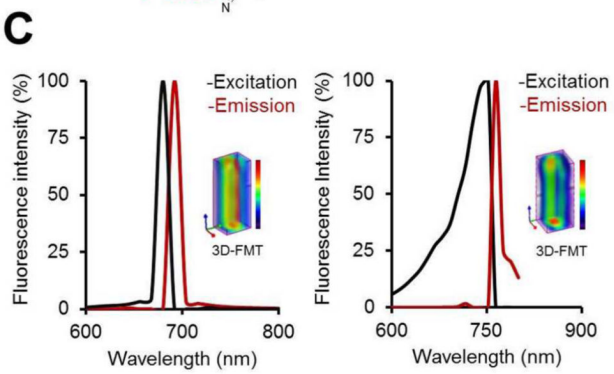

Figure 2. Chemical structure and characterization of the polymeric nanocarriers

A. Structure of the pHPMA-based polymeric drug carriers (P) coupled to vascular targeting ligands (where X = NGR, RGD or DRG (control)) and to a near-infrared fluorophore (DY-676). The peptide-free control copolymer P-CON was coupled to the near-infrared fluorophore DY-750. B. Physicochemical properties and peptide content of the four polymeric nanocarriers used in this study. C. Spectrophotometric analysis and FMT visualization of P-RGD (left) and P-CON (right).

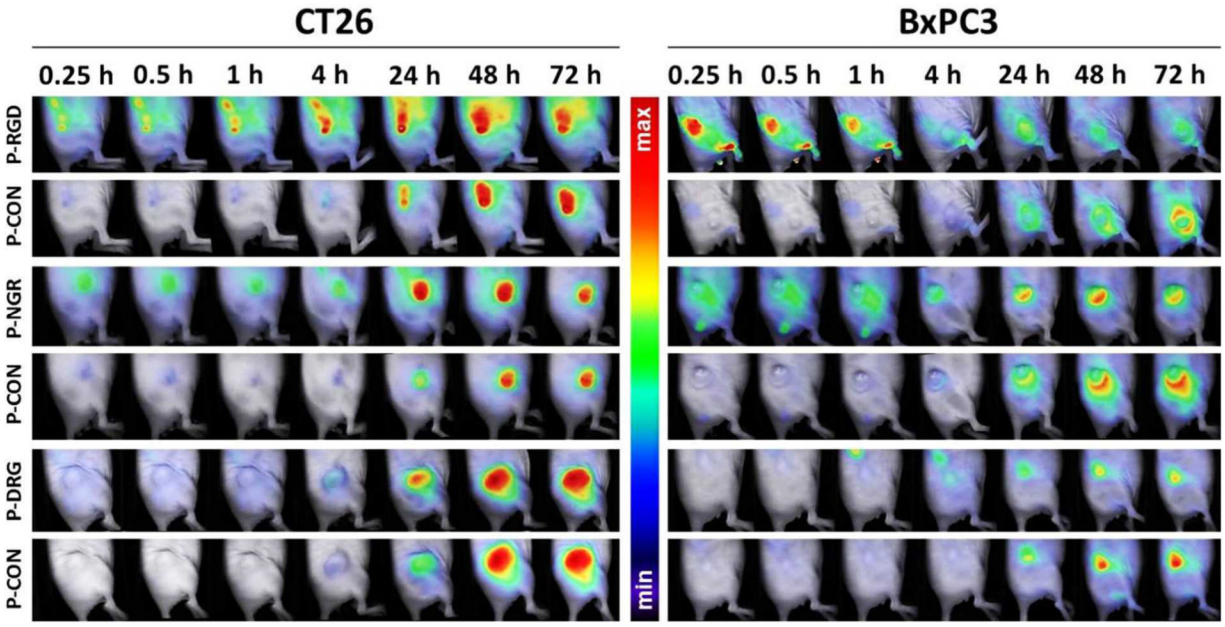

Figure 3. Fluorescence reflectance imaging (FRI) of passive vs. active (vascular) tumor targeting

Semi-quantitative 2D FRI analysis of the tumor accumulation of P-RGD, P-NGR, P-DRG and P-CON in CT26 and BxPC3 tumor-bearing mice. Early binding of the actively targeted probes P-RGD and P-NGR to tumor blood vessels could be observed in both CT26 and BxPC3 tumors, whereas the passively targeted probes P-DRG and P-CON presented with progressive EPR-mediated tumor accumulation.

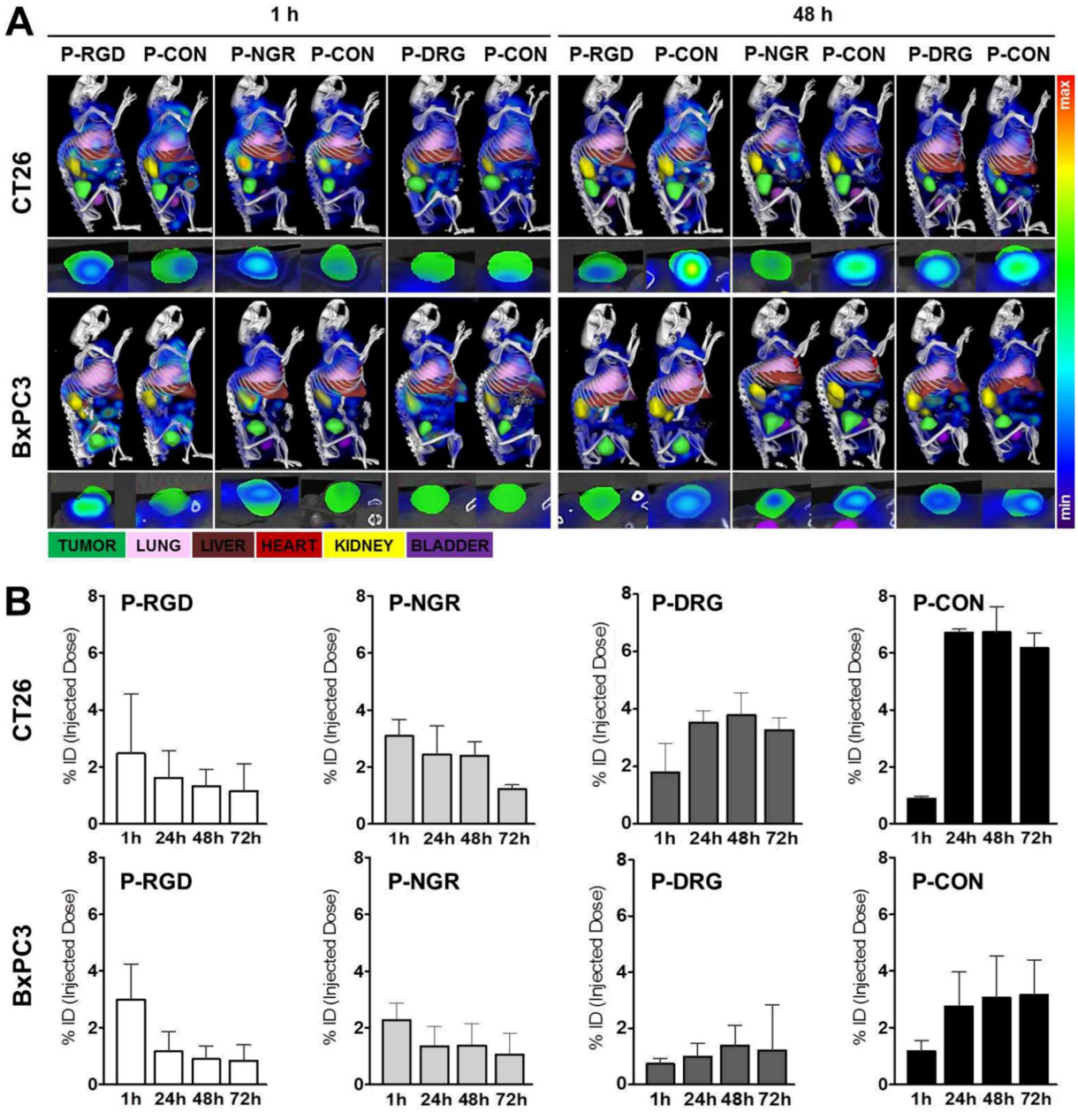

Figure 4. Hybrid computed tomography-fluorescence molecular tomography (CT-FMT) imaging of passive vs. active (vascular) tumor targeting

A. Representative 3D CT-FMT images of the biodistribution and the tumor accumulation of P-RGD, P-NGR, P-DRG and P-CON at early (1 h) and late (48 h) time points post i.v. injection in highly leaky CT26 and poorly leaky BxPC3 tumor-bearing mice. Tumors were pre-segmented using CT and are depicted in green. The images clearly demonstrate that active targeting to tumor blood vessels using RGD and NGR results in efficient early binding and rapid tumor accumulation, but is inferior to EPR-mediated passive targeting at later time points. B. Quantification of active (vascular) vs. passive tumor targeting using 3D CT-FMT, illustrating reasonably high tumor accumulation for P-RGD and P-NGR at early time points p.i., but significantly lower long-term levels in tumors as compared to P-DRG and P-CON. Values represent average ± SD.

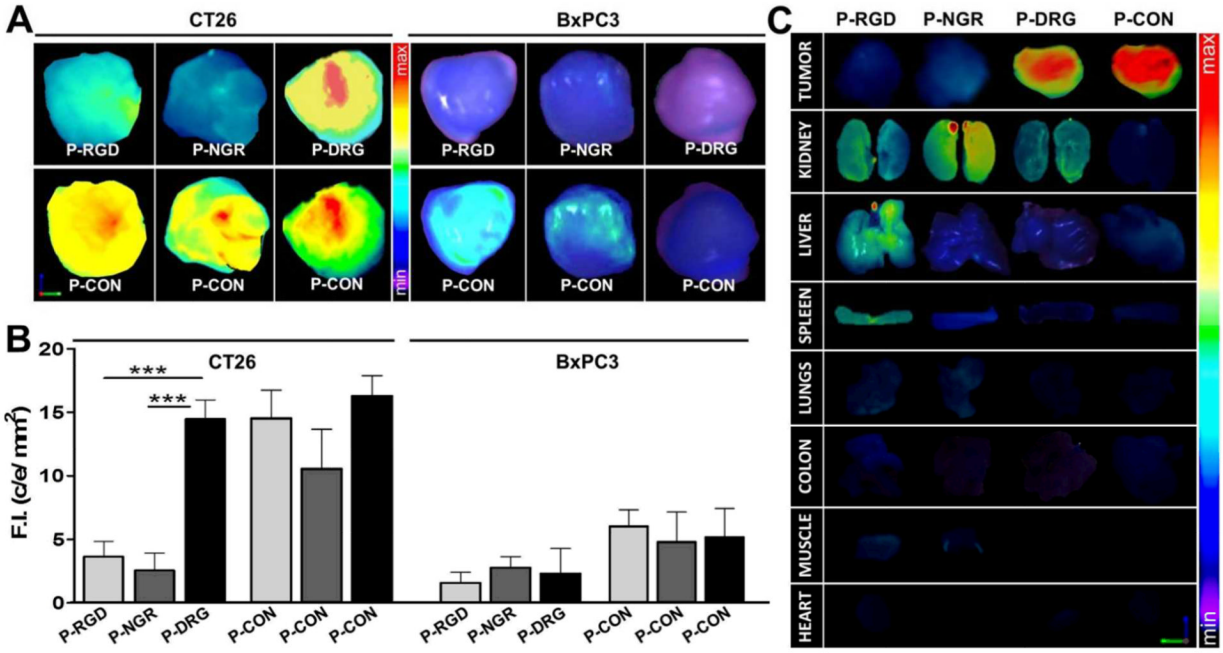

Figure 5. Ex vivo 2D FRI of tumor accumulation and biodistribution

A. Tumors were excised at 72 h p.i. and scanned using FRI, confirming the superiority of EPR-mediated passive over RGD- and NGR-based vascular tumor targeting. B. Quantification of P-RGD, P-NGR, P-DRG and P-CON accumulation in CT26 and BxPC3 tumors at 72 h p.i.. Fluorescence intensity was measured in counts/energy/area and is presented as average ± SD. * indicates $P<0.05$. C. Ex vivo biodistribution of the four polymeric nanocarriers, assessed using 2D FRI, exemplifying that peptide targeting leads to higher levels of off-target accumulation, in particular in liver and kidney.

Europe PMC Funders Author Manuscripts

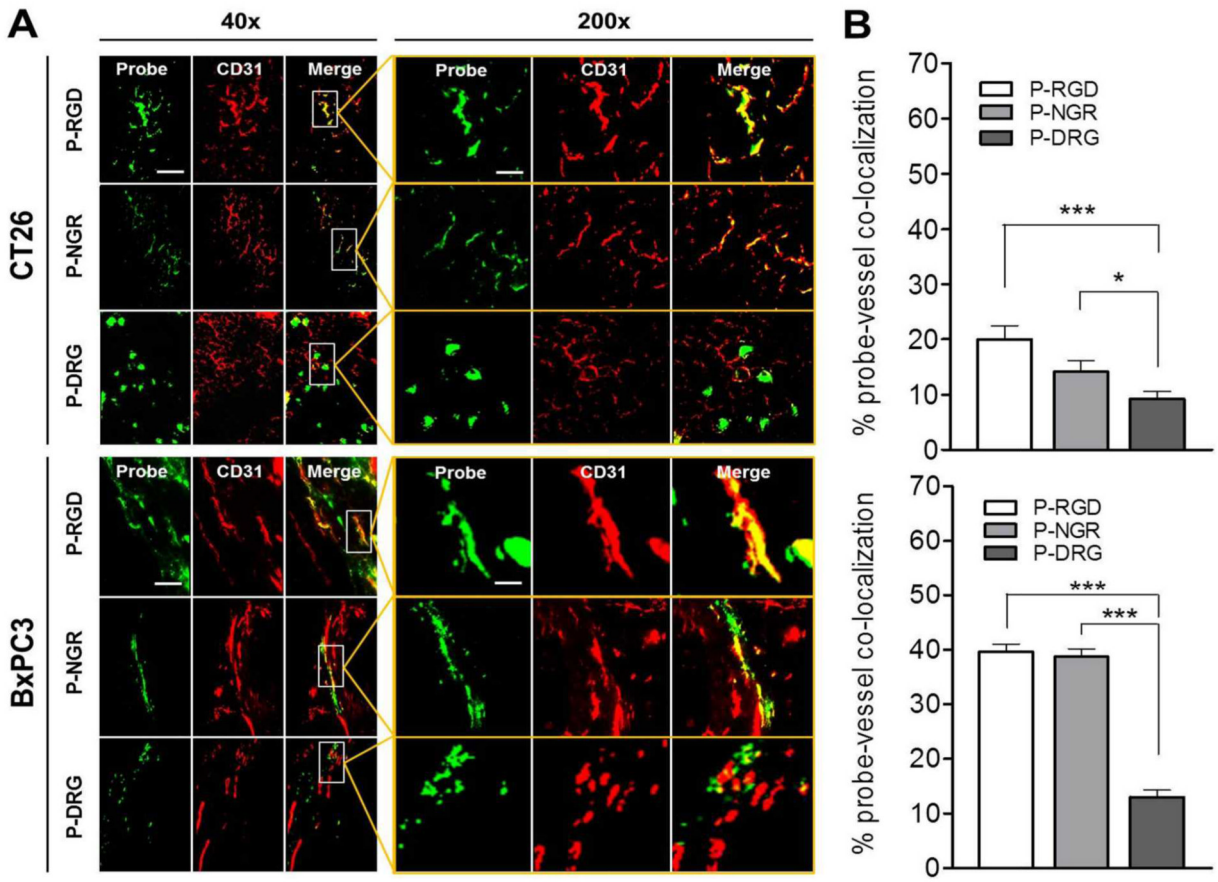

Figure 6. Ex vivo analysis of probe-vessel co-localization

A. Representative fluorescence microscopy images obtained at 72 h p.i., showing a higher degree of tumor blood vessel association for P-RGD and P-NGR than for P-DRG and P-CON, in both CT26 and BxPC3 tumors. Tumor endothelium was stained using antibodies against CD31. B. Quantification of the degree of probe-vessel co-localization. In total, 36 images were analyzed per condition. Values represent average ± SD. * P<0.05, *** P<0.005.

Europe PMC Funders Author Manuscripts

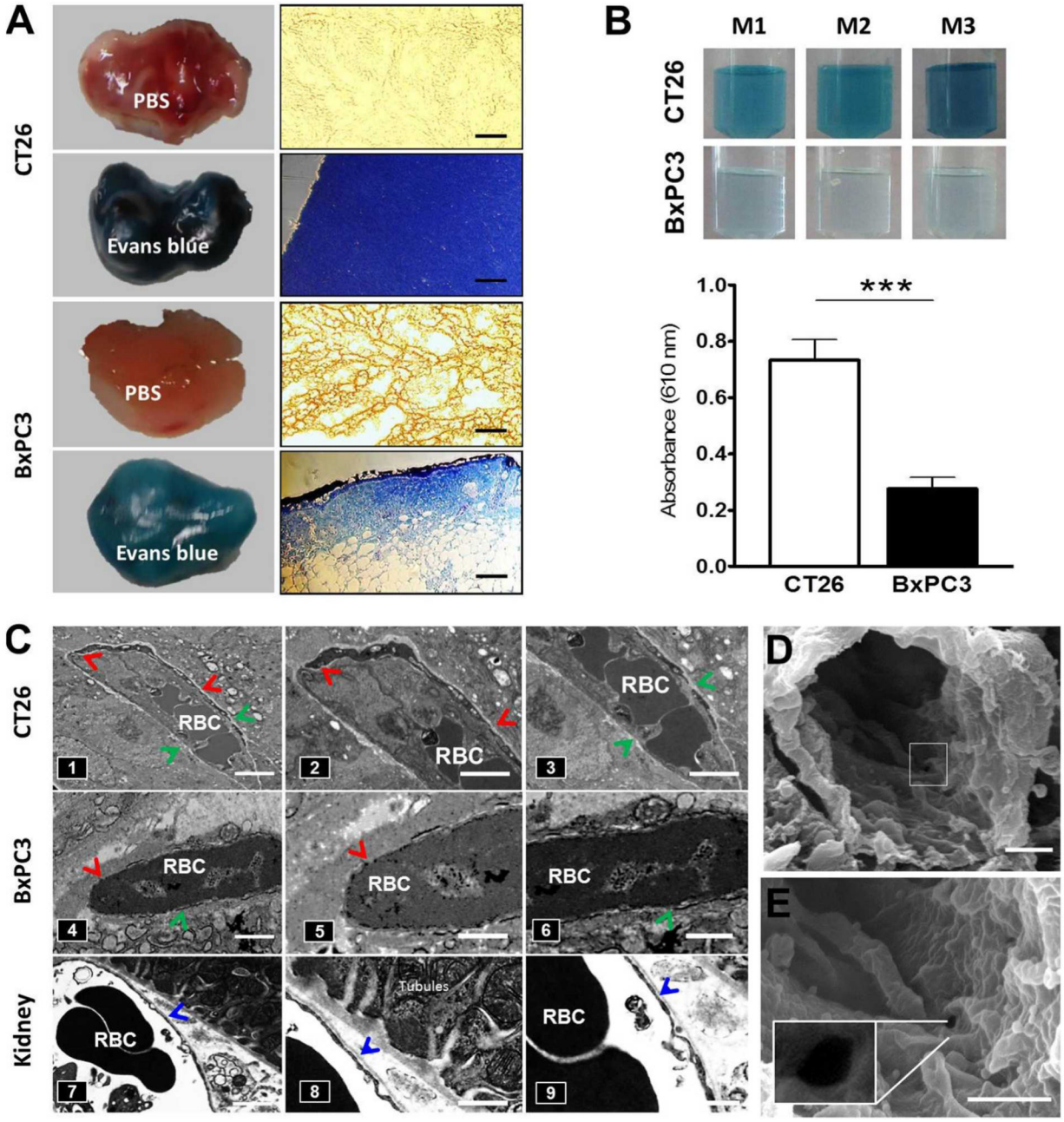

Figure 7. Assessment of vascular permeability

A. Qualitative images of Evans Blue Dye (EBD) extravasation in CT26 and BxPC3 tumors at 48 h after the i.v. injection of PBS or EBD (10 mg/kg). Bar: 20 μm. B. Tumor tissue extracts of EBD and their quantification, exemplifying a ~2.5-fold higher vascular leakiness in CT26 tumors. Values represent average ± SD. *** denotes $P<0.005$. C. High-resolution transmission electron microscopy (TEM) analysis of blood vessels in CT26 (1-3), BxPC3 (4-6) and kidney (7-9), demonstrating that capillaries in CT26 tumors presented with higher levels of endothelial misalignments (cf. panels 2 and 5: red arrowheads) and inter-endothelial gaps (cf. panels 3 and 6; green arrowheads) than capillaries in BxPC3 tumors. Blood vessels in kidney were intact and presented with a uniformly thick endothelium (blue

arrowheads). Scale bar: 2 μm. D-E. Scanning electron microscopy (SEM) analysis enabled the identification of defective endothelium in CT26 tumors, as exemplified by a distinct pore of ~150 nm in the capillary bed. Scale bar: 1 μm.

Europe PMC Funders Author Manuscripts